

SUPPLEMENTARY INFORMATION

Spectroscopic investigation into the design of solid-acid catalysts for the low temperature dehydration of ethanol

Matthew E. Potter,^{a*} Sivan V. Aswegen,^b Emma K. Gibson,^c Ian P. Silverwood^{c,d} and Robert Raja^{b*}

a) Department of Chemical and Biomolecular Engineering, Georgia Institute of Technology, 311 Ferst Drive, Atlanta, GA 30318, USA.

b) School of Chemistry, University of Southampton, University Road, Southampton, SO17 1BJ, United Kingdom; R.Raja@soton.ac.uk

c) UK Catalysis Hub, Research Complex at Harwell, Science and Technology Facilities Council Rutherford Appleton Laboratory, Harwell Science and Innovation Campus, Oxon OX11 0QX, United Kingdom.

d) ISIS Pulsed Neutron and Muon Facility, Science and Technology Facilities Council Rutherford Appleton Laboratory, Harwell Science and Innovation Campus, Oxon OX11 0QX, United Kingdom.

CONTENTS

SAPO-34 synthesis	Page S2
Silicon substitution mechanisms	Page S2
SAPO-34 Powder XRD	Page S3
FTIR experimental details	Page S3
Mass-spec data	Page S4
QENS experimental data	Page S4
QENS theoretical background	Page S5
Further QENS spectra and analysis	Page S6
References	Page S12

SAPO-34 synthesis

SAPO-34 synthesis was based on a procedure reported by us previously.^[1]

SAPO-34 synthesis involved initially adding 31.10 g of tetraethyl ammonium hydroxide (35 % in H₂O, Aldrich) to 15.10 g aluminium isopropoxide (Aldrich) and allowing the mixture to stir for 1.5 hr. 0.66 g of fumed silica (Aldrich) was added to the above solution, which was stirred for a further 30 minutes. A homogeneous solution of 8.52 g of phosphoric acid (85 % in H₂O, Aldrich) in 12.2 mL of water was added to the above solution which was stirred for a further 2 hr to obtain a gel with the composition 1.0Al:1.0P:0.15:Si:1.0TEAOH:50H₂O.

The contents of the gel were sealed in 2 Teflon-lined stainless-steel autoclaves, which were then transferred to a pre-heated, fan-assisted oven (WF-30 Lenton) that was set to the desired temperature of 200 °C, prior to the onset of the crystallization. The autoclave was heated at 200 °C under autogeneous pressure for 60 hr. The white solid product was collected by centrifuge, washed with approx. 100 mL deionised water, and dried in air (60 °C) overnight.

The as-synthesised sample was calcined in a tube furnace under a flow of air at 575 °C for 16 hr yielding a white solid.

For further characterization of this material we refer readers to reference 1.

Silicon substitution mechanisms

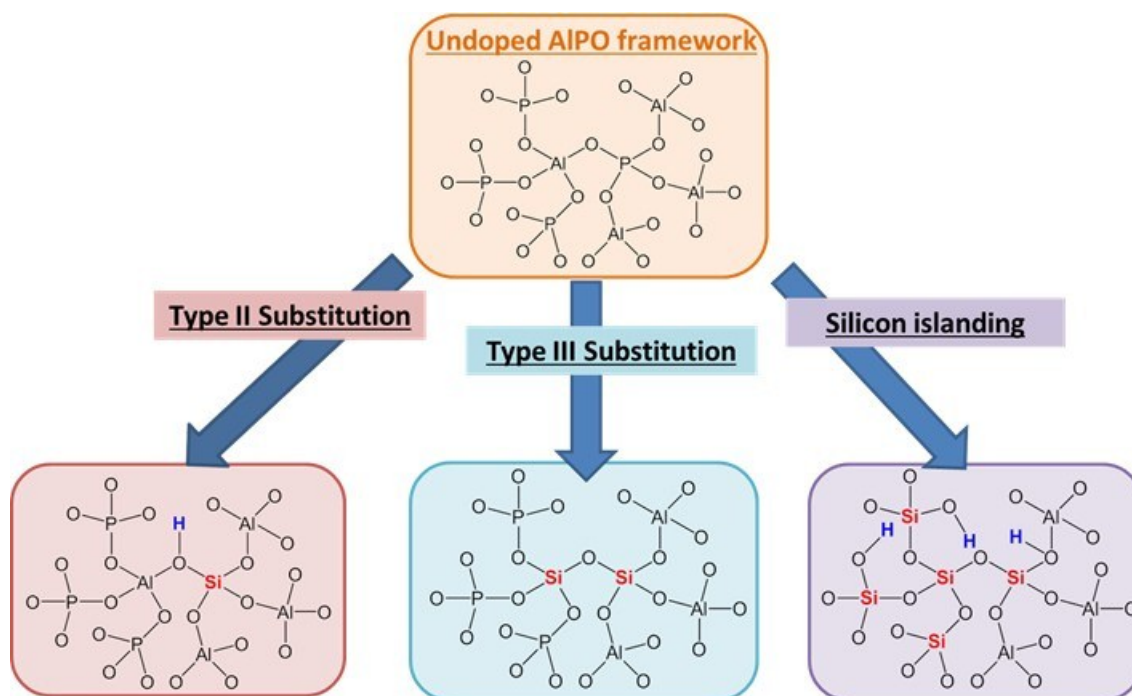


Figure S1: Possible silicon substitution methods into an AlPO framework.

SAPO-34 powder XRD

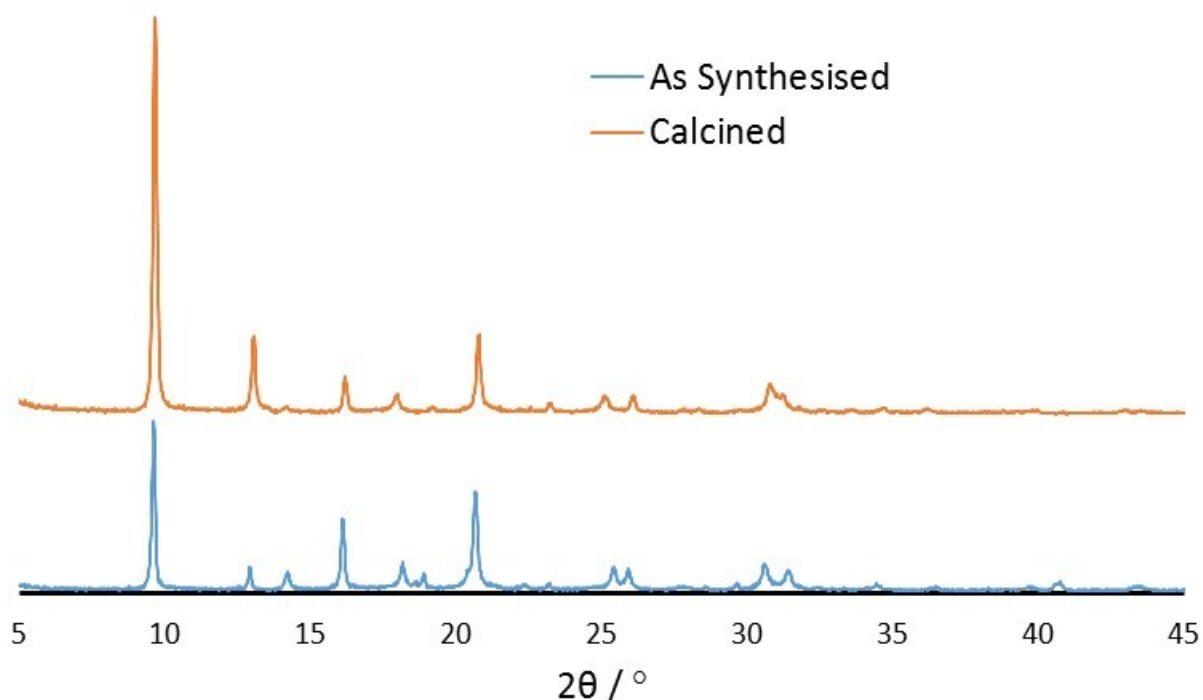


Figure S2: Powder XRD of SAPO-34, showing phase pure CHA structure in both the as synthesized (blue) and post-calcination (orange) forms.

FTIR experimental details

In situ diffuse reflectance infrared Fourier transform spectroscopy (DRIFTS) was performed in a Harrick high temperature DRIFTS cell fitted with ZnSe windows. The cell was attached to the Praying Mantis Optics and spectra collected with an Agilent Carey 680 FTIR spectrometer. The outlet gas was monitored using a Hiden Analytical, Quantitative Gas Analyser.

The sample was first heated in a flow of He (30 mLmin^{-1}) to 200°C at a ramp rate of 10°min^{-1} . After cooling to room temperature, under a 30 mLmin^{-1} flow of He, ten $1\mu\text{L}$ injections of ethanol were performed before heating to 400°C at a rate of 5°min^{-1} . DRIFTS spectra were collected after every injection and every 30s during the temperature ramp, taking 64 scans with a resolution of 4 cm^{-1} using the MCT detector.

Mass spectrometry data

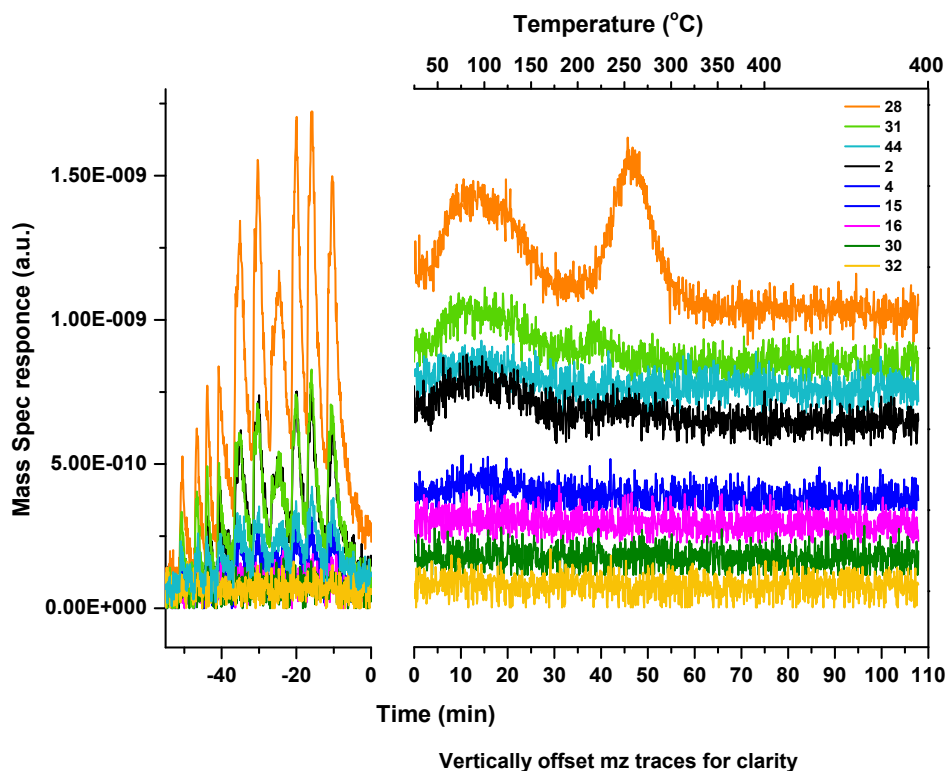


Figure S3: Mass-spec data showing the 10 doses of ethanol into the system (left) and the subsequent tracking of molecules as the *in situ* FTIR experiment progresses (right).

The $m/z = 28$ signal could be due to ethylene or CO. CO would be accompanied by the formation of H_2 ($m/z = 2$) due to the water-gas shift, which is clearly visible in the 50 – 150 °C signal, but is not significant in the 200 – 300 °C signal. As such we attribute the latter signal to primarily to ethylene formation.

QENS experimental details

SAPO-34 was dried overnight in a flow of 250 sccm He at 200 °C and thereafter transferred between sealed sample holders in an Ar glovebox. Sorbates were loaded by flowing He through a bubbler containing the organic material, and then the dried SAPO-34. Strong coherent scattering was experienced from the crystalline framework, as shown in Figure 1. The Bragg scattering features interfere with the quasielastic measurement, and data from these regions were discarded. Only the 13 detectors indicated in red in Figure 1 were used in the subsequent data treatment. This process ensured that the signal recorded was predominantly composed of the incoherent scattering from the sorbate and ameliorated the artefacts introduced through data subtraction. Data was recorded of the loaded samples at -263, 25, 50, 75, 100 and 125 °C. It was not necessary to group the 13 detectors to improve the signal to noise ratio. The spectra were rebinned in 0.0005 meV steps around the inelastic peak and in 0.001 meV steps from -0.2 to -0.1 and 0.1 to 0.2 meV. Outside this region, binning was 0.002 meV. The data was dotted using a resolution function, a delta function and two Lorentzians. The resolution function used was the data recorded of the ether-loaded SAPO-34 at base temperature (c. 10 K). Peak areas were constrained to be positive. Data

reduction was performed using Mantid.^[2] and fitting used DAVE.^[3] For the calculation of EISF values, the elastic peak of the empty SAPO framework was fitted with a delta function and the corresponding area subtracted from the fitted elastic component of the SAPO + absorbate system.

QENS theoretical background

When neutrons are scattered from a sample, they may undergo changes in energy and direction, which can be used as a probe of the sample. The scattering function (S) describes how the intensity of the scattered beam varies with energy transfer (ω) and scattering vector (Q) and is obtained after normalization of the raw data collected from the instrument. For quasielastic scattering, the energy transfer is of the same scale as diffusion processes and energy exchange between the neutron and sample results in a broadening of the measured elastic peak. The instrumental resolution determines the lowest energy transfer that can be determined, which corresponds to slow diffusion. As the quasielastic component broadens when higher energy transfer occurs, it becomes more difficult to distinguish from the background, and greater sensitivity is needed. This provides a practical limit to the greatest energy transfer, and fastest diffusion processes that may be measured.

Methods to improve resolution decrease sensitivity and vice versa, so instrumental design must be a compromise, and hence there is a window of energy that can be accessed. The resolution of the instrument can be measured experimentally by using a sample where there is no motion in the sample. This would ideally be at absolute zero, but in most cases measurement below 10 K is sufficient. The quasielastic peak centred on zero energy transfer can be represented as a convolution of the elastic component with quasielastic components for each motion present. The elastic component is represented as the convolution of a delta function and the measured resolution function. For a diffusion process, a Lorentzian peak is convolved. For free diffusion, the broadening of the quasielastic peak, or the width of the Lorentzian, is proportional to Q^2 . This is denoted either as FWHM (Full Width Half Maximum), or Γ (Half Width Half Maximum). The quasielastic technique measures neutrons that are scattered incoherently. Materials with long range order display Bragg peaks from coherent scattering at certain values of Q that interfere with the quasielastic measurement. Data from these regions can either be excised, or the coherent component may be subtracted.

The Singwi Sjolander model was used to analyze the trends in HWHM as a function of Q, observed in SAPO-34 ethanol and ether loaded systems:

$$HWHM(Q) = \frac{1}{6\tau_1 + Q^2 \langle r^2 \rangle / 6} \quad (1)$$

where $\langle r^2 \rangle$ is the mean-square jump distance and τ is the mean residence time. This is then translated into a diffusion coefficient (D) using the following equation:

$$D = \frac{\langle r^2 \rangle}{6\tau} \quad (2)$$

For systems where the FWHM is invariant of Q^2 , the diffusion coefficient is calculated thus:

$$D = \frac{1}{\tau}$$

(3)

Further QENS spectra and analysis

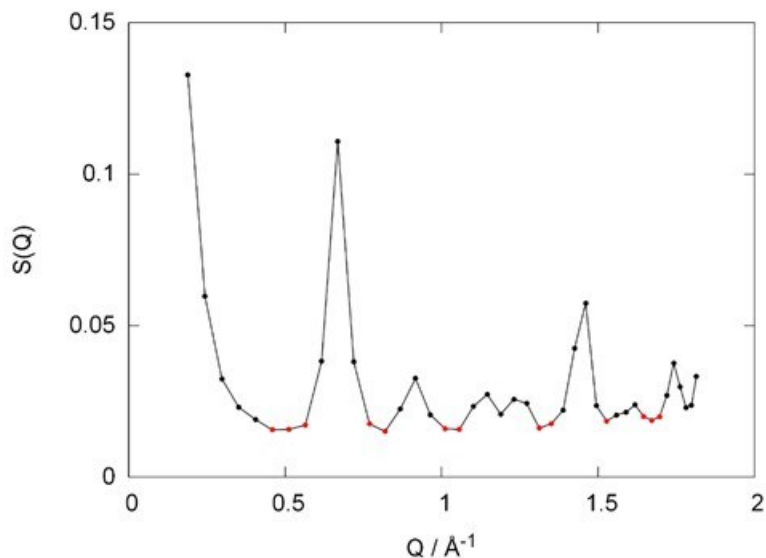


Figure S4: Scattering from the SAPO-34 framework showing the Bragg peaks. Further analysis was carried out using only the detectors shown in red to minimize the coherent scattering contribution.

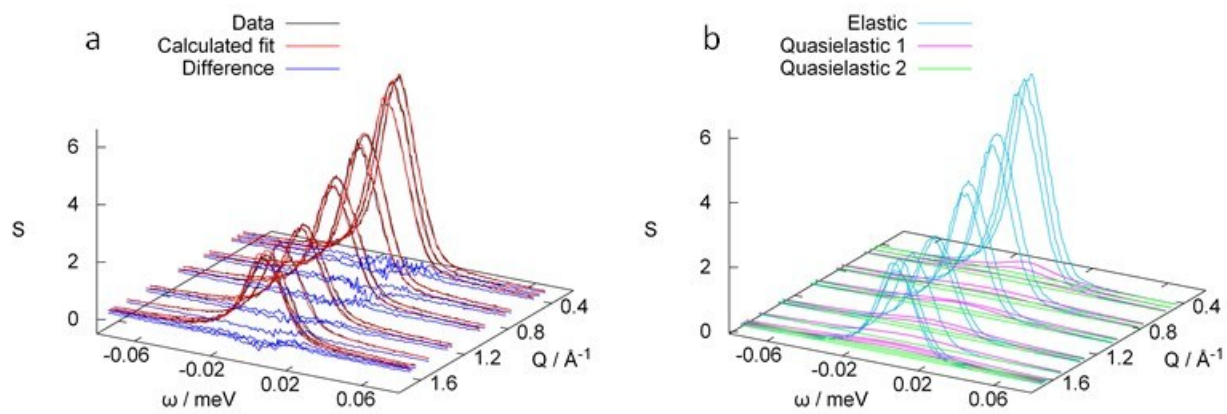


Figure S5: QENS spectra for SAPO-34 loaded with ethanol at 50 °C. a: Comparison of the fitted and experimental data, b: The individual fitted components.

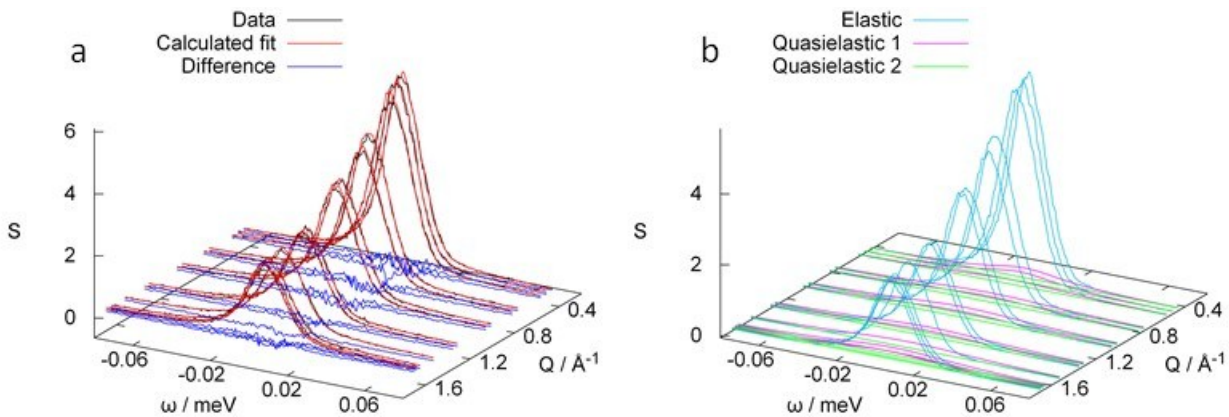


Figure S6: QENS spectra for SAPO-34 loaded with ethanol at 75 °C. a: Comparison of the fitted and experimental data, b: The individual fitted components.

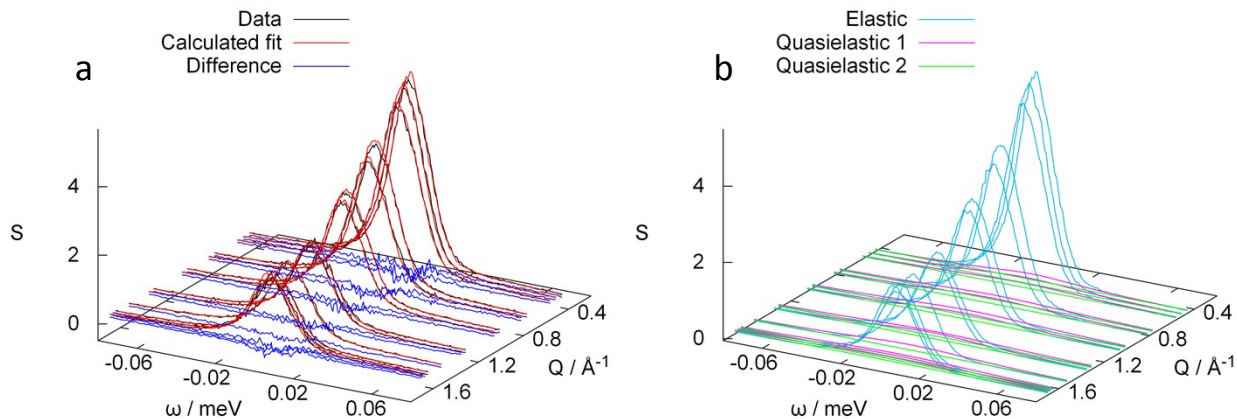


Figure S7: QENS spectra for SAPO-34 loaded with ethanol at 100 °C. a: Comparison of the fitted and experimental data, b: The individual fitted components.

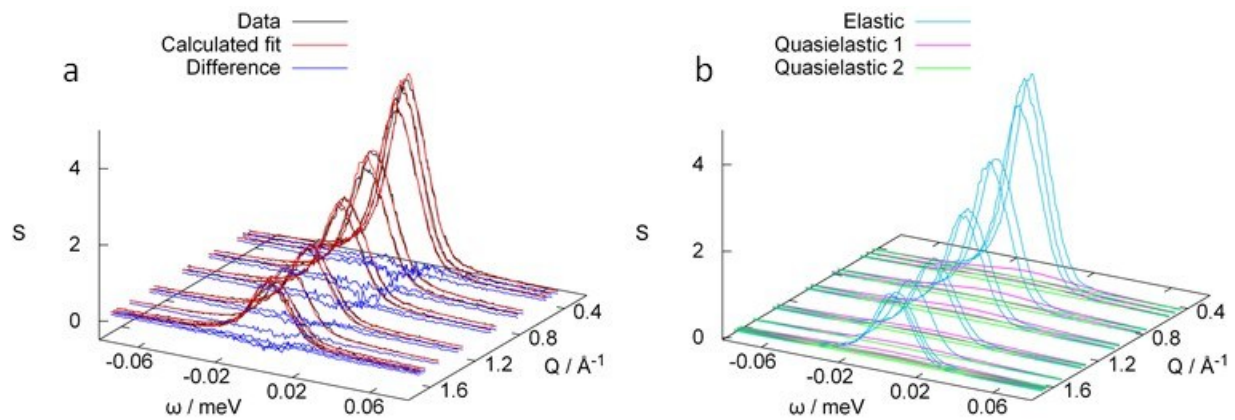


Figure S8: QENS spectra for SAPO-34 loaded with ethanol at 125 °C. a: Comparison of the fitted and experimental data, b: The individual fitted components.

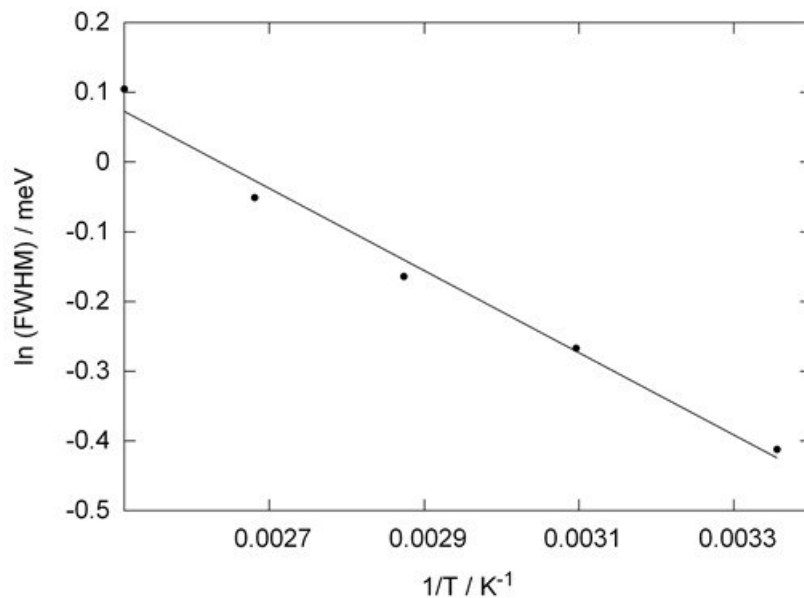


Figure S9: Arrhenius plot of the rotational process (L2) occurring in ethanol-loaded SAPO-34. The diffusion constant decreases with decreasing temperature, resulting in an activation energy of 5 kJ/mol.

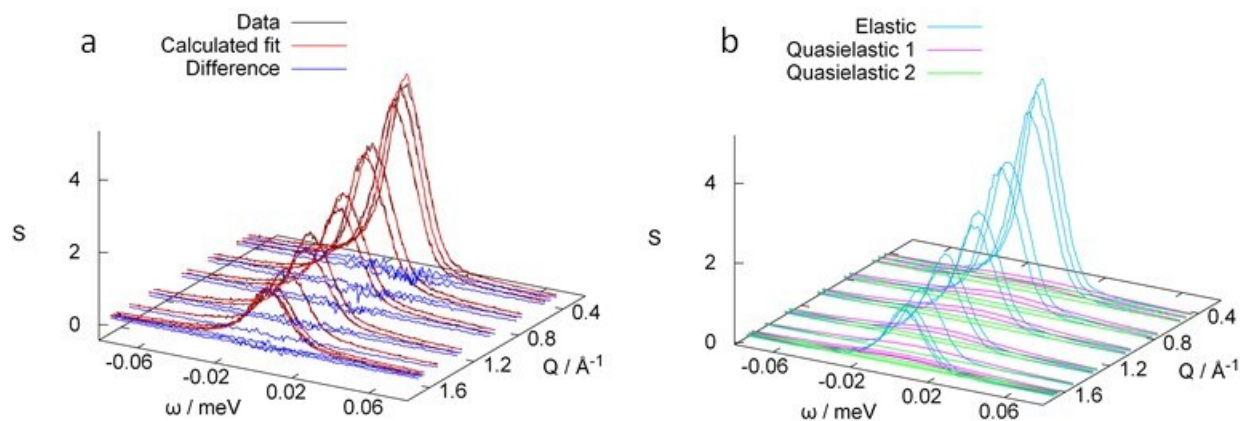


Figure S10: QENS spectra for SAPO-34 loaded with ether at 25 °C. a: Comparison of the fitted and experimental data, b: The individual fitted components.

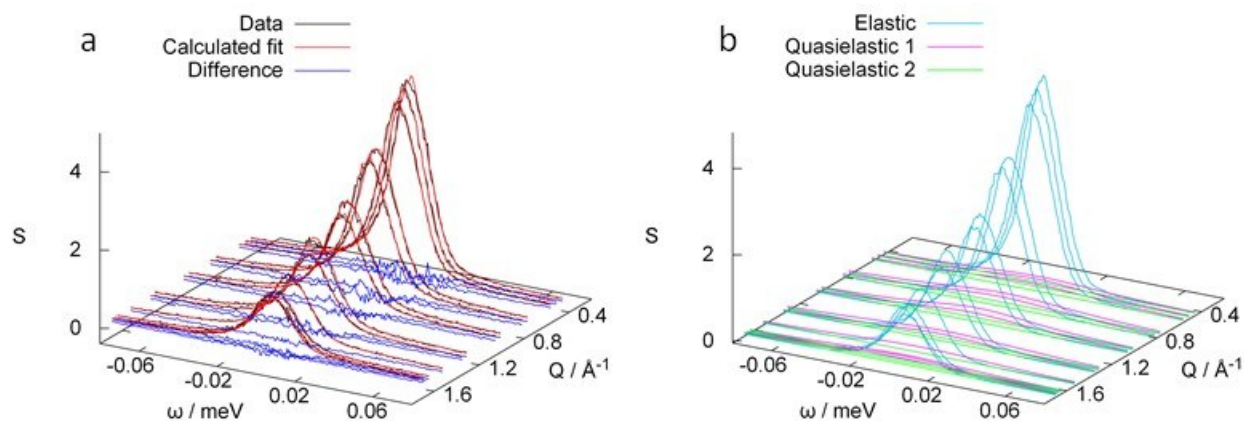


Figure S11: QENS spectra for SAPO-34 loaded with ether at 50 °C. a: Comparison of the fitted and experimental data, b: The individual fitted components.

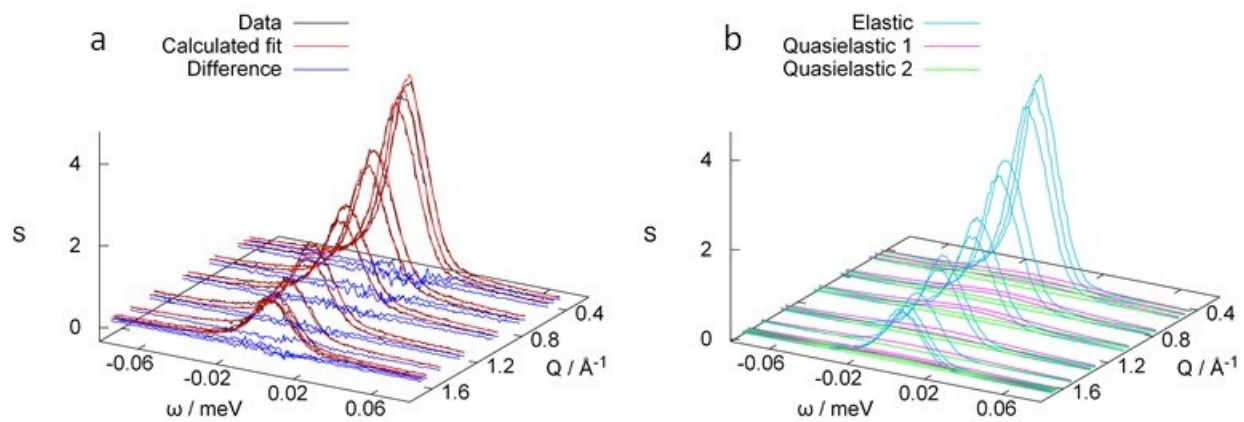


Figure S12: QENS spectra for SAPO-34 loaded with ether at 75 °C. a: Comparison of the fitted and experimental data, b: The individual fitted components.

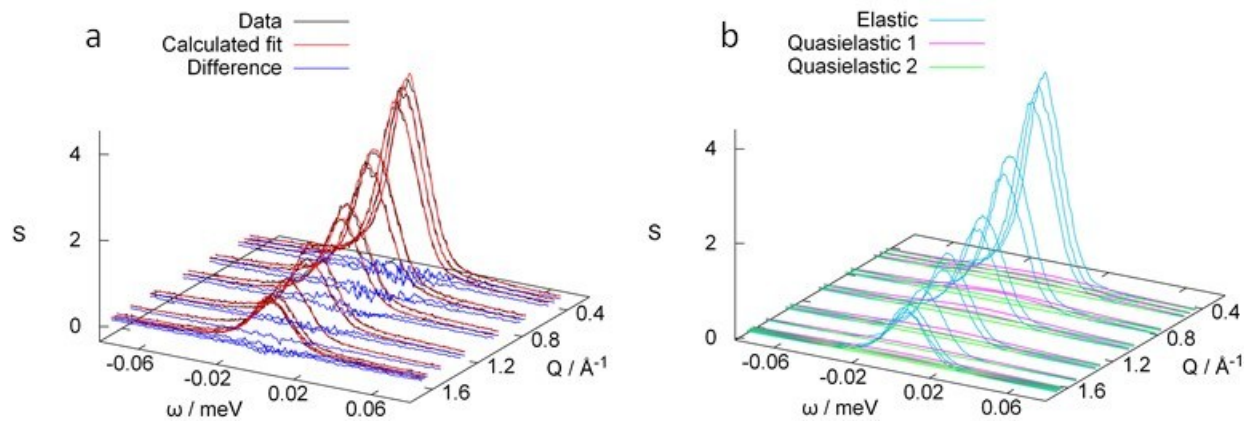


Figure S13: QENS spectra for SAPO-34 loaded with ether at 100 °C. a: Comparison of the fitted and experimental data, b: The individual fitted components.

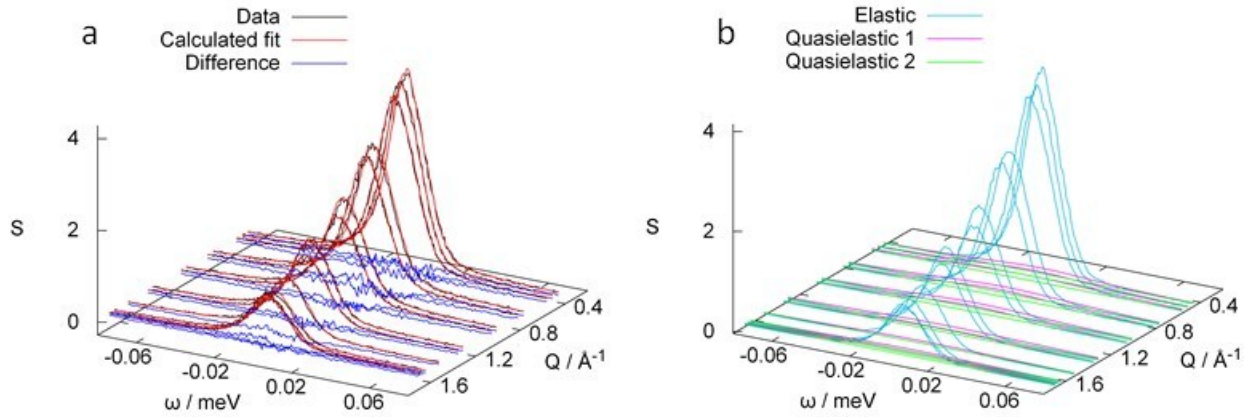


Figure S14: QENS spectra for SAPO-34 loaded with ether at 125 °C. a: Comparison of the fitted and experimental data, b: The individual fitted components.

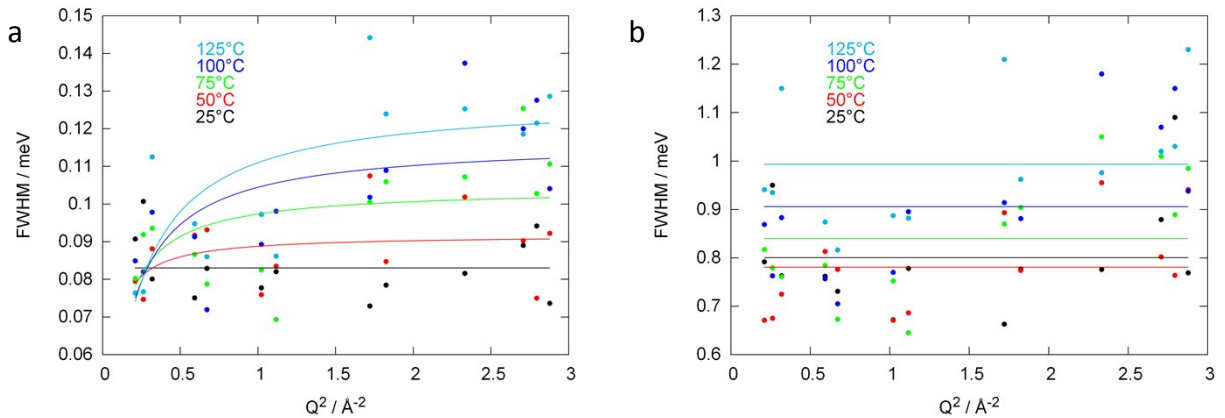


Figure S15: The influence of temperature on the relationship between the narrow Lorentzian (L3, a) which is fitted to a Singwi Sjolander jump model, and the broad Lorentzian (L4, b) that is fit as a constant value for the ether-loaded SAPO-34 system.

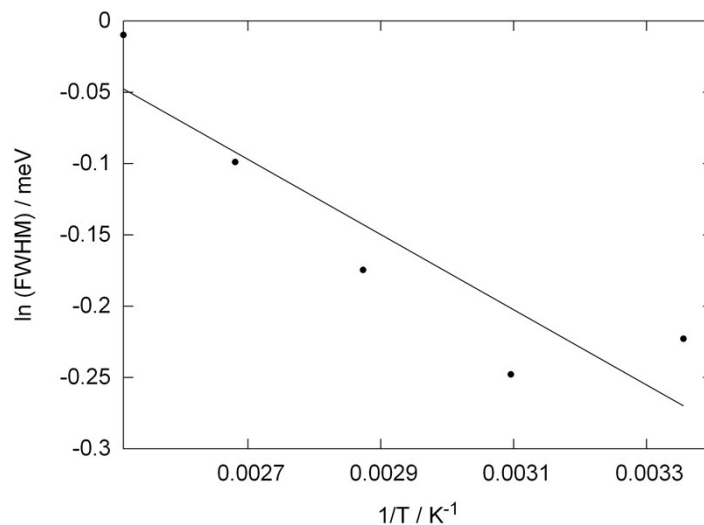


Figure S16: Arrhenius plot of the rotational process (L4) occurring in ether-loaded SAPO-34. The diffusion constant decreases with decreasing temperature, resulting in an activation energy of 2.2 kJ/mol.

References

- 1) M. E. Potter, M. E. Cholerton, J. Kezina, R. Bounds, M. Carravetta, M. Manzoli, E. Gianotti, M. Lefenfeld and R. Raja, *ACS Catal.*, 2014, **4**, 4161.
- 2) O. Arnold, J. C. Bilheux, J. M. Borreguero, A. Buts, S. I. Campbell, L. Chapon, M. Doucet, N. Draper, R. Ferraz Leal, M. A. Gigg, V. E. Lynch, A. Markvardsen, D. J. Mikkelsen, R. L. Mikkelsen, R. Miller, K. Palmen, P. Parker, G. Passos, T. G. Perring, P. F. Peterson, S. Ren, M. A. Reuter, A. T. Savici, J. W. Taylor, R. J. Taylor, R. Tolchenov, W. Zhou and J. Zikovsky, *Nucl. Instrum. Meth. A*, 2014, **764**, 156.
- 3) R. T. Azuah, L. R. Kneller, Y. Qiu, P. L. W. Tregenna-Piggott, C. M. Brown, J. R. D. Copley, and R. M. Dimeo, *J. Res. Natl. Inst. Stan. Technol.*, 2009, **114**, 341.